Articles

Proteolytic DNA for Mapping Protein−DNA Interactions†

Brian D. Schmidt and Claude F. Meares*

Department of Chemistry, University of California, One Shields Avenue, Davis, California 95616

Received July 17, 2001; Revised Manuscript Received December 10, 2001

ABSTRACT: We describe a technique to determine sites on proteins involved in protein−DNA interactions. DNA was synthesized via polymerase chain reaction (PCR) to produce four polynucleotide products with phosphorothioate nucleotides at the A, T, G, or C residues. Limited conjugation with the chemical protease FeBABE results in the surface of DNA being randomly labeled at the phosphorothioate sites with this protein-cleaving reagent. After formation of a protein−DNA complex, the proteolytic DNA can be activated to cleave the protein backbone at sites near the DNA. This technique was used to study the bacterial RNA polymerase/*lac*UV5 DNA open promoter complex, about which significant structural information is available. Cleavage sites on the two largest subunits of RNA polymerase, β and β', agree well with a recent model based on the crystal structure of the core enzyme $\alpha_2\beta\beta'$ [Naryshkin, N., Revyakin, A., Kim, Y., Mekler, V., and Ebright, R. H. (2000) *Cell 101*, 601−611]. The cleavage site present on α supports previous studies regarding DNA binding regions of the α subunit. Cleavage sites identified throughout the σ^{70} subunit help to orient it with respect to the open promoter complex.

The interactions of proteins with DNA play a major role in biological processes such as gene transcription or DNA replication. Methods are available for the analysis of these interactions (*1*), but most focus on identifying the regions of DNA involved. Experimental strategies to map protein surfaces at sites of interaction with DNA are less well developed.

Protein footprinting—in which proteins are cut by reagents in solution, such as proteases or iron-EDTA—has been used for this purpose (*2*−*4*). However, changes in specific bands can be difficult to interpret because protein gel electrophoresis neither provides single-residue resolution, nor differentiates cuts due to binding interactions from those brought about by conformational changes (*5*). Likewise, protein cross-linking has been employed to study DNA−protein interactions (*6*, *7*), but presents its own challenges. Often, the site of the cross-link is difficult to identify. To overcome this problem, extensive experiments relating cross-links in regions of a protein to numerous individual base pairs in the DNA have been used to assign protein−DNA contacts (*6*).

Previously we have studied protein−protein interactions by cleavage of the polypeptide backbone using the tethered cleavage reagent FeBABE[1] (*8*−*12*). A particularly successful strategy involves placing FeBABE on the surface of a protein at random points and cleaving adjacent proteins in a complex (*11*, *12*). We reasoned that mapping DNA binding sites on proteins could be achieved by placing FeBABE on the surface of DNA, thus transforming DNA into a chemical protease.

Substituting a nonbridging oxygen on the phosphodiester DNA backbone with a sulfur results in a phosphorothioate oligodeoxynucleotide. As shown in Figure 1, we used PCR to create a set of four DNA fragments (*13*), each containing a *5′*-thiophosphoryl nucleotide at the A, T, G, or C positions. Under appropriate conditions (*14*), a small percentage of the nucleophilic sulfur atoms on the phosphodiester backbone react with FeBABE to produce a collection of DNA molecules conjugated at various positions. Each of these fragments contains a limited number of FeBABE molecules scattered across the surface at different locations. If these conjugated DNA fragments are taken as a set, as shown in Figure 1B,C, almost any part of the DNA surface has the possibility of containing an FeBABE molecule. Thus, upon forming a protein−DNA complex, every region of the protein surface near the DNA should be susceptible to polypeptide backbone cleavage. Due to the extension of FeBABE from the surface of the DNA, initiation of the cleavage reaction is expected to produce cut sites at the periphery of the protein−DNA binding site.

As shown in Figure 1C, regardless of which dNTPαS is used, cleavage reagents are expected to be similarly scattered across the DNA surface. The reach of protein cleavage is expected to be approximately 15 Å from the sulfur of the

† This work was supported by Research Grant GM25909 to C.F.M. from the National Institutes of Health.

* Address correspondence to this author at the Department of Chemistry, University of California, One Shields Ave., Davis, CA 95616-5295. Telephone: 530-752-0936. Fax: 530-752-8938. E-mail: cfmeares@ucdavis.edu.

[1] Abbreviations: dNTPαS, deoxynucleoside 5′-triphosphate (dNTP) in which a nonbridging oxygen is replaced with a sulfur at the α-phosphorus position; FeBABE, iron-(*S*)-1-(*p*-bromoacetamidobenzyl)-EDTA; PBS, 0.14 M NaCl, 0.0027 M KCl, 0.010 M Na_2HPO_4, 0.0018 M KH_2PO_4, pH 7.2; PBST, PBS containing 0.05% Tween-20.

10.1021/bi015582r CCC: $22.00
Published on Web 03/12/2002

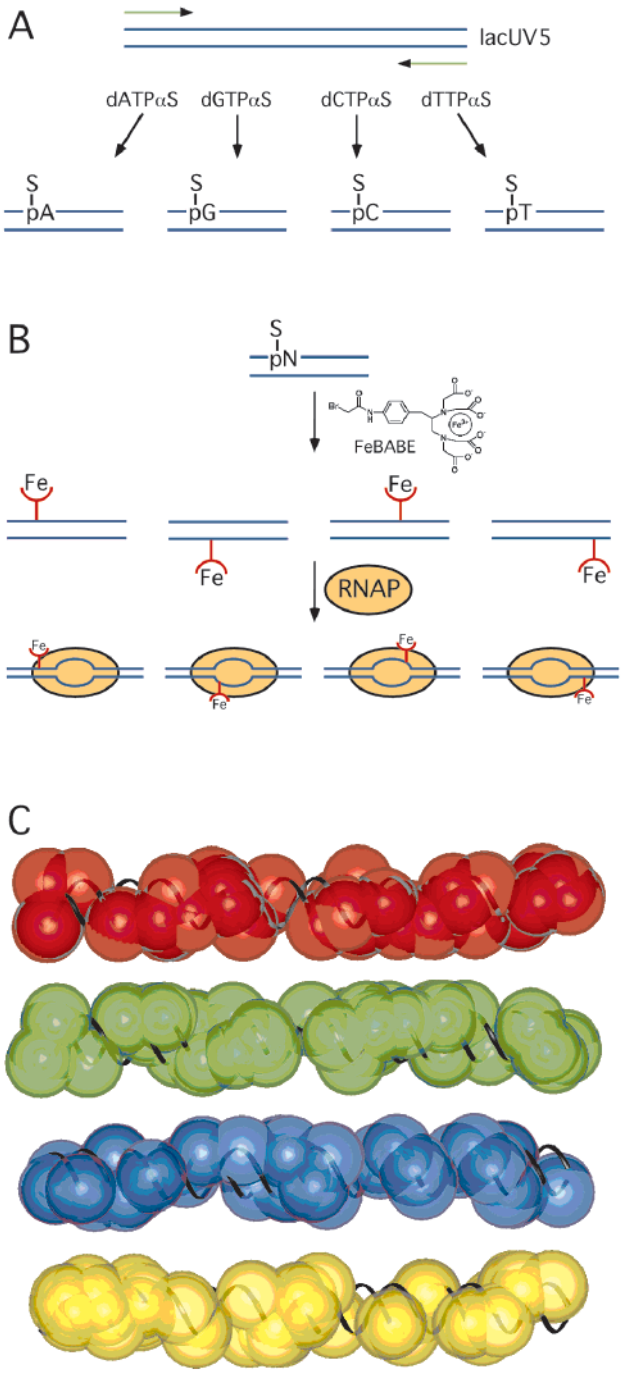

FIGURE 1: (A) Production of DNA in which either A, C, G, or T residues contain phosphorothioate sulfur. *lac*UV5 DNA is amplified in four separate reactions from template plasmid. (B) The figure shows one of the four (N) being lightly conjugated to produce a random labeling of FeBABE on the DNA backbone. With regard to the actual experiment, only a small percentage of the total number of residues are being labeled. After formation of the protein−DNA complex, cleavage of the protein occurs where it is proximal to an FeBABE. (C) A fragment from −50 to +20 of *lac*UV5 is illustrated with each A (red), T (green), G (blue), or C (yellow) nonbridging oxygen rendered as a 15 Å sphere to represent the reach of FeBABE and the minimum potential coverage on the DNA surface.

phosphorothioate to the periphery of the chelate, but may be greater depending on the extent of hydroxyl radical diffusion from the iron chelate (*15*).

To evaluate this method of mapping protein−DNA interactions, the multisubunit enzyme RNA polymerase (RNAP) was employed. RNAP is responsible for the transcription of DNA; binding of DNA to the RNAP holoenzyme (whose subunit composition is $\alpha_2\beta\beta'\sigma^{70}$) to create a transcriptionally active "open" promoter complex is a crucial stage in this process. The structure of *Thermus aquaticus* (Taq) core RNAP ($\alpha_2\beta\beta'$, *16*), an open promoter complex model placing DNA onto the Taq structure (*6*), and the structure of a fragment of the σ^{70} protein from *E. coli* (*17*) provide a basis to map and evaluate the contact sites between lacUV5 and RNAP.

MATERIALS AND METHODS

Materials. Phosphorothioate nucleotides were purchased from Amersham Pharmacia Biotech. FeBABE was prepared according to (*18*). Ascorbic acid (vitamin C, microselect grade) was purchased from Fluka and hydrogen peroxide (Ultrex grade) from J. T. Baker. Reactibind neutravidin microplates were purchased from Pierce. Goat anti-mouse λ-alkaline phosphatase conjugate was purchased from Southern Biotechnology Associates, Inc. *p*-Nitrophenyl phosphate tablets and rifampicin were purchased from Sigma.

Preparation of Phosphorothioate DNA. The 228 bp fragment of pLAC12 (−157 to +71) containing the *lac*UV5 promoter (*19*) was synthesized by PCR amplification using the appropriate dNTPαS, and the remaining dNTPs as substrates. The PCR conditions for amplification include 200 μM of each dNTP or dNTPαS, 2 mM $MgCl_2$, 4.3 nM pLAC12 template, 5 units/100 μL of Taq DNA polymerase, and 700 nM of each primer. PCR was run for 31 cycles of 94 °C; 1 min (cycle 1: 5 min), 57 °C; 45 s, 72 °C; 2 min (cycle 31: 10 min), and purified using a QIAquick PCR purification kit (Qiagen) followed by ethanol precipitation.

*lac*UV5 was also engineered to contain deoxynucleoside 5′-thiophosphoryl (phosphorothioate) bases at only the ends of the fragment. 20 and 21 nucleotide primers containing phosphorothioate cytosine nucleotides with sequences identical to those used above were purchased (Operon), and PCR amplification was performed using only normal dNTPs.

FeBABE Conjugation. Conjugation reactions were performed in 20 mM MOPS, 2 mM EDTA, pH 7, containing 6 mM FeBABE and 1.6 μM phosphorothioate DNA (≈0.2 mM phosphorothioate). After 3 h of incubation at 50 °C (*14*), excess FeBABE was removed by a micro bio-spin column (Bio-Rad) equilibrated with 15% glycerol in cleavage buffer (10 mM MOPS, 120 mM NaCl, 10 mM $MgCl_2$, 1 mM EDTA, pH 7.9). Conjugates were stored at −70 °C until use. For control experiments, non-phosphorothioate *lac*UV5 DNA was treated in the same manner.

Conjugation Yield. To determine the approximate number of FeBABE molecules that were conjugated to each double-stranded *lac*UV5 fragment, a competitive ELISA was performed as illustrated in Figure 2. Fifty microliters of 1.5 μM biotin−FeBABE conjugate (*20*) was added to each well of a neutravidin-coated 96-well microtiter plate and incubated at 37 °C for 1 h. After the plate was washed 3× with PBST (*21*), 10 dilutions of Fe-(*S*)-*p*-nitrobenzyl-EDTA and the DNA conjugate were performed over a range from 90 μM to 0.3 nM Fe-(*S*)-*p*-nitrobenzyl-EDTA and from 0.8 μM to 3 pM DNA conjugate, respectively. Then 25 μL of each dilution, followed by 25 μL of 10 nM anti-chelate antibody CHA255 (*22*), was added to each well, and the plate was

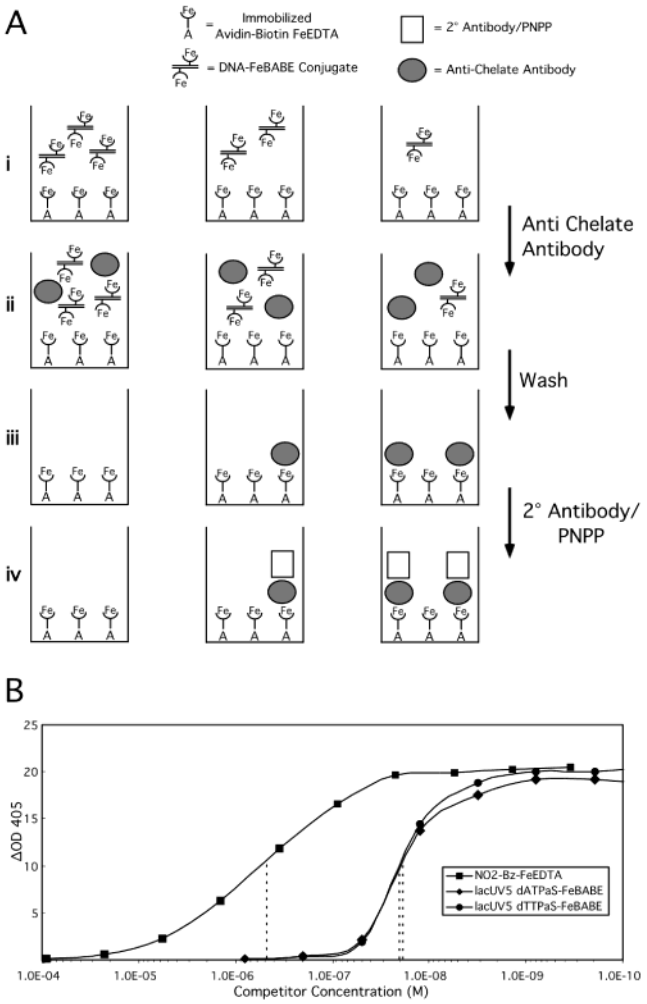

FIGURE 2: (A) A competitive ELISA assay was used to determine the number of FeBABE molecules per double-stranded DNA fragment. (i) Decreasing amounts of DNA−FeBABE conjugate are added to microtiter wells, which contain a constant amount of FeEDTA immobilized to the surface. (ii) A constant amount of the anti-chelate antibody CHA255 is added to all the wells. (iii) After competition between the DNA−FeBABE conjugate and the immobilized Fe-chelate, the wells are washed, leaving an increasing amount of CHA255 bound in the well. (iv) A secondary antibody conjugate specific for CHA255 is added to all wells, followed by washing and the addition of PNPP to produce a yellow color, which is monitored at 405 nm via a microplate reader. (B) A graph plotting the change in absorbance at 405 nm vs the concentration of competitor is shown. Dashed lines show the corresponding concentrations at 50% saturation.

shaken for 2 h at room temperature. After being washed 3× with PBST, 50 μL of a 1/2000 dilution of anti-mouse λ-alkaline phosphatase was added to each well and incubated for 2 h at room temperature. The plate was washed 3× with PBST and rinsed with 10 mM diethanolamine, 0.5 mM $MgCl_2$, pH 9.5. One hundred microliters of *p*-nitrophenyl phosphate (PNPP) dissolved in diethanolamine was added to each well. The plate was centrifuged for 2 min at 1000*g*, and kinetic measurements were taken at 405 nm with a microplate reader over 1 h. All assays were done in triplicate. The rate of change in absorbance was plotted against the concentration of competitor. The number of chelates per DNA was derived by dividing the concentration of the Fe-(*S*)-*p*-nitrobenzyl-EDTA standard at 50% saturation by the concentration of DNA in the DNA−FeBABE conjugate, as shown in Figure 2B.

Transcription Assay Using Phosphorothioate DNA. Single-round runoff transcription assays were performed on both conjugated and unconjugated *lac*UV5 phosphorothioate DNA (*23*−*25*). Briefly, an open complex was formed by the addition of phosphorothioate template DNA to holoenzyme and incubating at 37 °C for 15 min. Transcription was initiated by addition of heparin and a mixture of NTP's, including [α-^{32}P]UTP, and allowed to proceed at 37 °C for 5 min. Reactions were quenched, precipitated, and resolved by PAGE. The 71 nt RNA transcript was visualized on a Molecular Dynamics Storm phosphorimager. Transcriptional activities relative to non-phosphorothioate DNA were measured by densitometry and averaged for triplicate experiments.

Cleavage of RNAP Holoenzyme by FeBABE-lacUV5. A mixture of RNAP holoenzyme (1 μM final) and FeBABE-conjugated *lac*UV5 (0.5 μM final) was incubated at 37 °C for 20 min in cleavage buffer. Heparin (50 μg/mL final) was added 3 min before cleavage reactions were initiated (*26*). A 50 mM solution of ascorbate containing 10 mM EDTA (titrated to approximately pH 7 with dilute NaOH) was made in advance and stored at −70 °C. A 50 mM solution of peroxide containing 10 mM EDTA was prepared just before use. After incubation, the cleavage reactions were initiated by adding the ascorbate (5 mM final) and peroxide (5 mM final) solutions, followed by vortex mixing. The reaction times varied from 1 to 5 min at 37 °C. Reactions were quenched by adding 0.25 volume of 5× sample application buffer [312.5 mM Tris-HCl, pH 8.2, 10% (w/v) lithium dodecyl sulfate, 5% (v/v) 2-mercaptoethanol, 50% glycerol, 25 mM EDTA, 0.05% (w/v) bromophenol blue], immediately frozen in liquid nitrogen, and stored at −70 °C. For reactions done in the presence of rifampicin, RNAP holoenzyme was incubated with rifampicin (10 μM final) for 15 min at 37 °C prior to the addition of DNA. The fragments were separated by SDS−PAGE, electrophoretically blotted onto PVDF membranes, and visualized with affinity-purified subunit terminus-specific antibodies as described by Greiner et al. (*27*).

Assignments of Cleavage Site Fragments. Cleavage sites on α, β, β', and σ^{70} were assigned by comparison to chemical digests generated from the same protein, and the number of residues in each fragment was measured from mobility (*28*). 2-Nitro-5-thiocyanatobenzoate (NTCB) and cyanogen bromide (CNBr) digests were performed essentially as described by Owens et al. (*10*). Hydroxylamine digests, which cleave between asparagine and glycine residues, were initiated by the addition of hydroxylamine cleavage buffer (8 M urea, 3 M NH_2OH, pH 9.5), incubated at 42 °C for 2−4 h, and quenched with 2-mercaptoethanol (140 mM final) at 37 °C for 15 min (*29*, *30*). *N*-Chlorosuccinimide (NCS) digests, which cleave at tryptophan residues, were initiated by the addition of NCS (3 mM final) in NCS cleavage buffer (27.5% acetic acid, 4.68 M urea), incubated for 1 h at room temperature, and stopped with a 4-fold molar excess of *N*-acetyl-L-methionine (*31*). All cleavage fragments were visualized and assigned using a Fluor-S MultiImager with Quantity One software (Bio-Rad). Experiments were independently performed and analyzed 3 times. The standard deviation of the triplicate measurements was calculated for each cut site, and was between ±3 and ±11 residues.

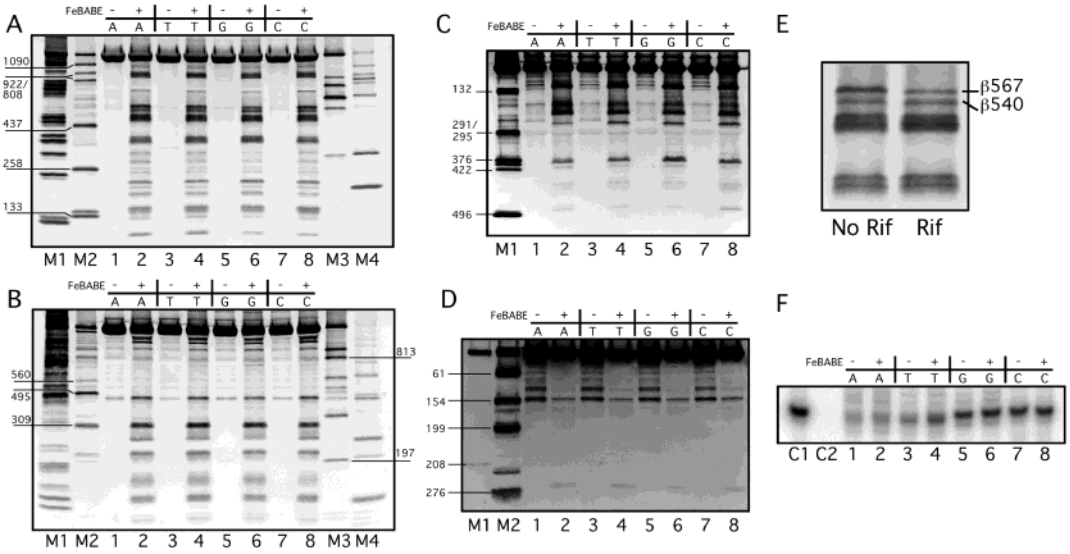

FIGURE 3: (A−E) Protein fragments generated from FeBABE conjugated phosphorothioate *lac*UV5 cleaving RNAP holoenzyme. Immunostained western blots of SDS−PAGE detecting either (A,E) β or (B) β' using antibodies against the N-terminus of the respective subunit, or detecting (C) σ^{70} and (D) α using antibodies against their C-termini. Lanes 1, 3, 5, and 7 correspond to unconjugated *lac*UV5 phosphorothioate DNA modified at the A, T, G, and C bases, respectively. Lanes 2, 4, 6, and 8 correspond to FeBABE conjugated *lac*UV5 DNA phosphorothioate modified at the A, T, G, and C bases, respectively. (A) and (B) lanes M1, M2, M3, and M4 correspond to respective CNBr, NH_2OH, NTCB, and NCS chemical digests of the respective subunit. (C) Lane M1 is an NTCB digest of wt σ, 376C, 396C, 422C, and 496C single cysteine mutants. (D) Lanes M1 and M2 correspond to the respective NH_2OH and NTCB chemical digests of α. (E) Cleavage reaction without rifampicin and in the presence of 10 μM rifampicin. (F) *lac*UV5 directed transcriptional activity of phosphorothioate DNA. All lanes contained RNAP holoenzyme except lane C2, which contained only RNAP core enzyme and was used as a negative control. Control lanes C1 and C2 contained nonphosphorothioate *lac*UV5. Lanes 1−8 use the same DNA as lanes 1−8 described above. Transcriptional activity relative to nonphosphorothioate DNA (lane C1) are as follows for lanes 3−10: A, 23%; A-FeBABE, 30%; T, 39%; T-FeBABE, 52%; G, 73%; G-FeBABE, 77%; C, 69%; C-FeBABE, 66%. The standard deviation for triplicate measurements was calculated for each transcript to yield an overall precision of 5−15%.

RESULTS

FeBABE-Modified lacUV5. A 228 bp segment of *lac*UV5 was synthesized by PCR to contain a 5′-thiophosphoryl residue at either A, T, G, or C, and subsequently conjugated with FeBABE. As determined by competitive ELISA, there are approximately 20−40 chelates conjugated to each double-stranded *lac*UV5 promoter, representing 18−35% of the phosphorothioate nucleotides or 4−9% of the total residues in the DNA. Control experiments showed that the cleavage pattern produced by the proteolytic DNA was not dependent on the level of conjugation. Control conjugation experiments using *lac*UV5 DNA with no phosphorothioate residues showed background labeling of 1−3 chelates per DNA, which when used in cleavage experiments did not produce detectable cleavage of the holoenzyme (data not shown).

To evaluate the ability of RNAP to transcribe RNA from phosphorothioate-modified and FeBABE-conjugated DNA, transcription assays were performed (Figure 3F). RNA was transcribed from all four phosphorothioate DNA templates. A significant decrease in RNA transcription was observed when the DNA template contained phosphorothioates at the A or T positions, even before FeBABE was attached. It is possible that since the −10 (TATAAT) and −35 (TTGACA) promoter elements of the DNA are rich in A and T bases, substitution with phosphorothioate nucleotides at A and T positions could have a significant impact on the ability of RNAP to bind the promoter, and thus on the transcription of RNA. Conjugating FeBABE to the DNA had a minimal effect on the ability of RNAP to transcribe from the promoter DNA.

Cleavage of RNAP Holoenzyme by lacUV5-FeBABE Conjugate. Site-specific cleavage of β and β' by *lac*UV5 produced the greatest number of cleavage fragments, followed by σ^{70} and α. Western blots of SDS−PAGE gels showing cleavage of β, β', σ^{70}, and α are shown in Figure 3. Cut sites are summarized in Figure 4 and listed in Table 1 (published as Supporting Information). As shown in Figure 3, all four sets of conjugated *lac*UV5 DNA, corresponding to conjugation at either the A, T, G, or C nucleotides, displayed the same cleavage fragments within experimental error. This is consistent with the relatively uniform coverage of the DNA surface expected for all four phosphorothioate templates, as shown in Figure 1C.

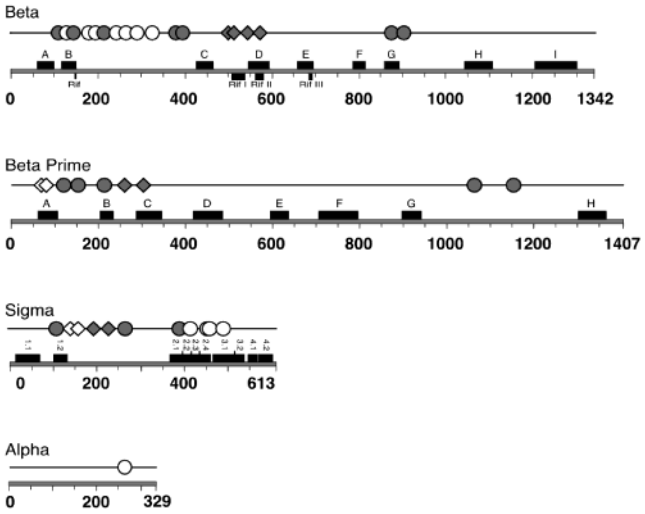

FIGURE 4: Summary of the cut sites on β, β', σ^{70}, and α. Shaded symbols correspond to bands with greater intensities. Diamonds indicate those cut sites that are also cut by reagents at the ends of the *lac*UV5 DNA, as discussed in the text.

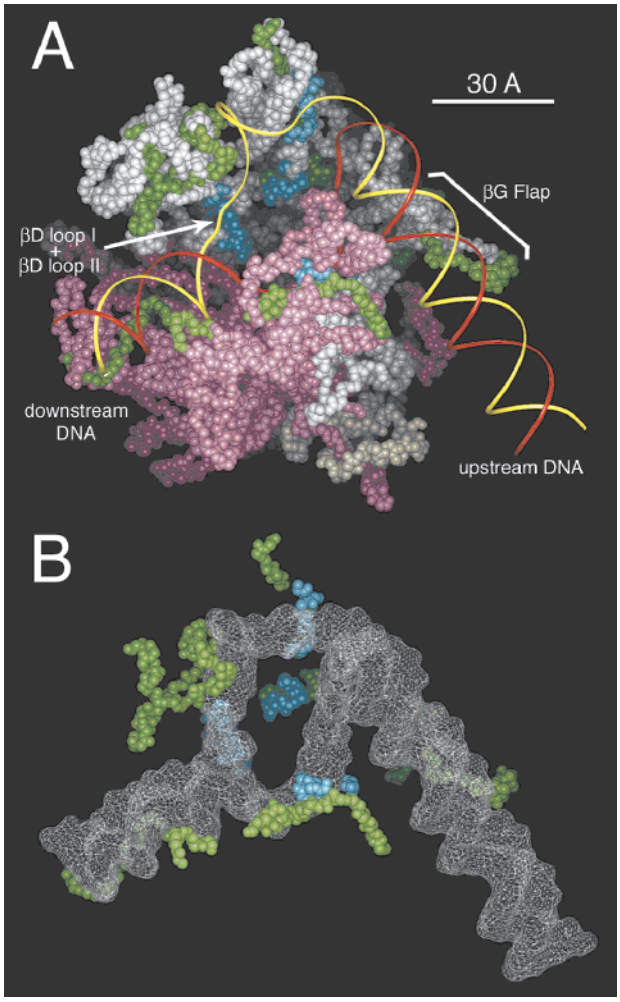

FIGURE 5: (A) A view looking into the active site of the DNA/RNAP open promoter complex. RNAP is displayed as CPK spheres of the backbone only. Regions are colored as follows: β, white; β', purple; α and ω, tan; nontemplate DNA strand, yellow; template DNA strand, red; cut sites, green; cut sites also due to end-labeled DNA, aqua. (B) Only β and β' cut sites and DNA (rendered as a surface) are displayed. Colors are identical to those used in (A).

The RNAP/DNA open complex was challenged with heparin to eliminate RNAP/DNA complexes not due to promoter-specific complexes (*26*). It is possible that some nonspecific RNAP/DNA complexes (involving binding of RNAP at the DNA ends) may be resistant to heparin (*6*). To identify cleavage fragments that are a result of end-bound complexes, FeBABE was conjugated to DNA containing phosphorothioate nucleotides located at only the ends of the DNA. The cleavage sites resulting from reactions with this DNA and the RNAP holo complex were a subset of the fragments normally seen when only the middle of the DNA is labeled. Omitting these cut sites (illustrated in Figure 4, Table 1, and colored aqua in Figure 5) still produces a complete, consistent description of where the DNA interacts with the holoenzyme. The sites cut by both end- and middle-labeled DNA may correspond to regions of the protein critical to DNA binding, regardless of the detailed nature of the complexes.

DISCUSSION

Recently, two models of bacterial RNAP/DNA complexes have been proposed (*6*, *7*) representing different stages of the transcription process. Korzheva et al. have presented a model of the transcription elongation complex, and Naryshkin et al. have proposed a model of the RNAP-promoter open complex. Based on extensive cross-linking data of the RNAP−*lac*UV5 promoter open complex, Naryshkin et al. (*6*) have placed DNA into the *Taq* RNAP core enzyme structure (*16*). In Figure 5A,B, we compare the results of our cleavage reactions, also performed on the RNAP−*lac*UV5 promoter open complex, to the latter model. The sites cut by the proteolytic DNA are highlighted on the model and are all in close proximity to the DNA as modeled by Naryshkin et al.

Several specific cleavage sites within the RNAP holoenzyme are described below. Two cut sites are located on what is referred to as the flexible βG flap (Figure 5A) (*7*, *16*). This flap, encompassing *E. coli* β residues 805−951, is an independent structural domain that appears to be flexibly connected to RNAP. It has been hypothesized that this flexibility may enable it to change conformations, possibly in the transition from a promoter-specific open complex to an elongation complex (*16*). Cut site 898 is located on part of the flap, which is thought (*6*) to interact directly with the major groove of the upstream duplex DNA, from approximately position −22 to position −28.

The open promoter complex differs from the transcription elongation complex because it is an earlier intermediate in the transcription process; although a stable transcription bubble has been formed, NTPs are not being consumed for the production of RNA. The elongation complex is actively transcribing RNA and moving along the DNA duplex.

It is thought that within the transcription elongation complex there is a hingelike rotation of two segments of β onto the DNA/RNA hybrid (*7*). This closing of the RNAP "jaws" is thought to bring two loops, βD loop I (Figure 5A) centered at residue 543 and βD loop II (Figure 5A) centered at residue 568, into close proximity with the DNA, possibly to have specific roles within the transcription bubble. Both of these loops were cut by the proteolytic *lac*UV5 DNA, at residues 540 and 567, respectively (labeled in Figure 3E), indicating they may play important roles in the open complex as well.

βD loop II also seems to be important for the binding of the antibiotic rifampicin. This loop contains rifampicin resistance mutations (*7*, *32*), and the rifampicin−RNAP crystal structure (*33*) shows rifampicin directly abutting the base of the loop. As our results show in Figure 3E, cleavage reactions performed in the presence of rifampicin show a marked decrease in the intensity of the cut site centered at residue 567 in βD loop II.

Another interesting example is the cut site located near residue 264 on the α subunit. This site lies on the N-terminal end of helix 1 of the α subunit C-terminal domain (αCTD) structure (*34*). It has been determined that two regions of the αCTD are important for DNA binding: region 1 corresponding to helix 1, and region 2 corresponding to a loop between helices 3 and 4 (*35*). Arg265, which is part of helix 1, has been shown to be critical with respect to UP element dependent transcription (*35*, *36*). Although the *lac*UV5 upstream sequence does not contain an UP element (*37*), it is clear from our results and others (*6*) that the α subunit does contact the DNA to some degree. Our data

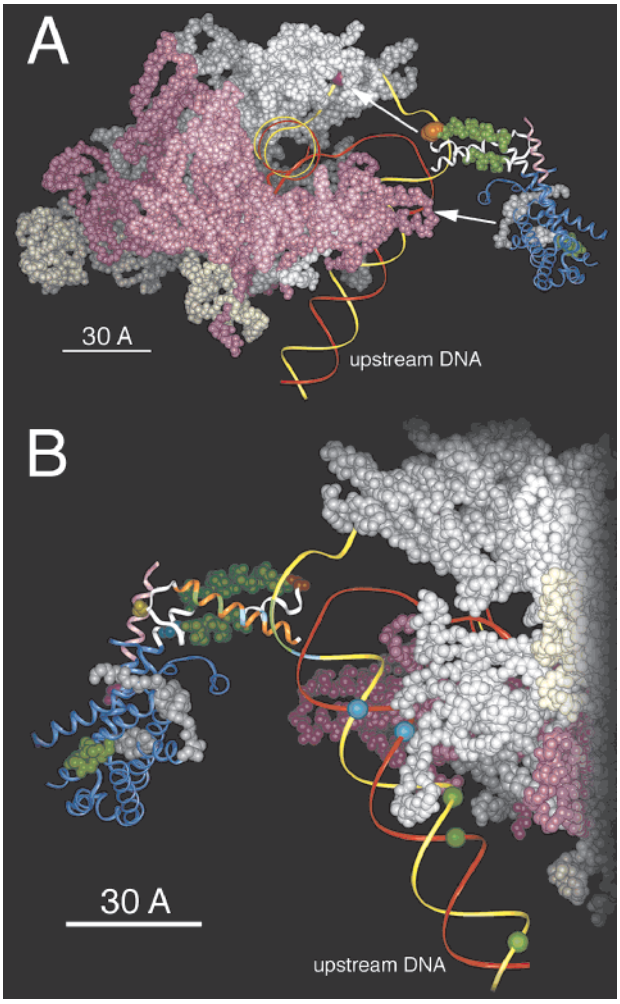

FIGURE 6: σ^{70} oriented with respect to the RNAP open promoter complex. Colored regions: β, white; β', purple; α and ω, tan; nontemplate DNA strand, yellow ribbon; template DNA strand, red ribbon; σ^{70}, blue ribbon; cut sites on σ^{70}, green and gray spheres (gray cut sites are localized sites between region 1.2 and 2.1 as described under Discussion); region 1.2, pink ribbon; region 2, white ribbon. (A) Colored regions: Cys396, orange spheres; +1 base on the nontemplate strand, purple sphere. (B) rotated 180° around the *y*-axis with respect to (A). Colored regions: helix 14, orange; −10/−11 bases of the nontemplate strand, green ribbon; −12 base, aqua ribbon; Tyr430 and Trp433 of σ^{70}, green ribbon; Gln437 and Thr440 of σ^{70}, aqua ribbon. Data from (*9*) are also shown. Aqua spheres on DNA represent single cysteine cut sites from Cys496, and green spheres on DNA represent single cysteine cut sites from Cys581. Single cysteine residues rendered as spheres on σ^{70} are colored as follows: Cys132, purple; Cys376, aqua; Cys396, orange; Cys422, yellow.

corroborate these previous results, which indicate Arg265 as the most important residue in the αCTD for DNA binding.

Because σ^{70} is present within the RNAP open promoter complex, it was also cleaved by the proteolytic DNA. Detecting cut sites on σ^{70} from *lac*UV5 revealed sites in regions 1.2, 2.1, 2.2, 2.4, and 3.1, and the region between 1.2 and 2.1. We did not observe cuts in region 4, perhaps due to limitations in sensitive detection of small fragments by western blotting, or possibly because appropriately positioned chemical nucleases inhibit binding. Six of the cut sites (near residues 141, 159, 229, 264, 392, and 411) can be modeled onto the crystal structure of the σ^{70} subunit fragment (*17*), and are shown in Figure 6.

In the case of RNAP, we and others have previously proposed models of how σ^{70} interacts with DNA in an open promoter complex (*9*, *38*). The new cut sites on σ^{70} described here and cleavage data we have published previously (*9*, *10*) make it possible to further evaluate proximity relationships with the core enzyme. Conformational changes are known to occur within σ^{70} and RNAP (*39*, *40*). For this reason, the separate structures do not fit together directly, and prevent us from positioning σ^{70} into an exact location within the core enzyme. As shown in Figure 6A, we have placed the available σ^{70} structure just outside the RNAP/DNA model provided by Naryshkin et al., leaving the coordinates of each individual structure unaltered. Arrows illustrate the proximity relationships between the σ^{70} subunit and the open complex as described below.

As constraints for positioning in Figure 6, we relied most heavily on the cut sites located in regions 2.1 and 2.2, the cut sites between regions 1.2 and 2.1 that were localized in one region of σ^{70}, and cleavage data indicating residue 396 of σ^{70} is near position +1 of the nontemplate strand of DNA (*9*). These data place region 2 of σ^{70} within the cleft of the enzyme, which includes the single-stranded region of DNA (the transcription bubble). The remainder of σ^{70} lies outside the cleft, with one face of σ^{70} (including localized cut sites between regions 1.2 and 2.1) along the duplex DNA just upstream of the transcription bubble.

The resulting orientation, illustrated in Figure 6B, suggests the relationship of σ^{70} helix 14 to the nontemplate DNA strand. Results of genetic studies, based on DNA-melting experiments and affected transcriptional activity, indicate σ^{70} helix 14 residues Tyr-430 and Trp-433 are near the DNA bases −11/−10 and helix 14 residues Gln-437 and Thr-440 interact with the DNA base −12 (*17*, *41*−*45*). These results led to a proposal (*17*) that places Gln-437 and Thr-440 upstream relative to Tyr-430 and Trp-433. Owens et al. (*9*) argued that the genetically identified interactions might be separated in time during the transcription process, and modeled the DNA of the open complex oriented in the opposite direction. A significant feature of the model of Naryshkin et al. is that the transcription bubble bends strongly away from the upstream DNA duplex. The existence of such a DNA bend makes it possible to reconcile the data in the earlier reports: as shown in Figure 6B, this bend locates helix 14 in an orientation opposite to that proposed in (*9*), and in agreement with the previous proposal (*17*).

ACKNOWLEDGMENT

We thank Todd Corneillie for advice concerning the ELISA assay, and Saul Datwyler, A. J. Chmura, and Donald Corson for helpful discussions. We thank Richard Ebright and Seth Darst for providing pdb coordinates of RNAP/DNA complexes.

SUPPORTING INFORMATION AVAILABLE

Table 1 lists the assignments of the sites at which cleavage occurred on α, β, β', and σ^{70}. This material is available free of charge via the Internet at http://pubs.acs.org.

REFERENCES

1. Guille, M. J., and Kneale, G. G. (1997) *Mol. Biotechnol. 8*, 35−52.

2. Heyduk, E., and Heyduk, T. (1994) *Biochemistry 33*, 9643−9650.
3. Baichoo, N., and Heyduk, T. (1999) *J. Mol. Biol. 290*, 37−48.
4. Frank, O., Schwanbeck, R., and Wisniewski, J. R. (1998) *J. Biol. Chem. 273*, 20015−20020.
5. Datwyler, S. A., and Meares, C. F. (2000) *Trends Biochem. Sci. 25*, 408−414.
6. Naryshkin, N., Revyakin, A., Kim, Y., Mekler, V., and Ebright, R. H. (2000) *Cell 101*, 601−611.
7. Korzheva, N., Mustaev, A., Kozlov, M., Malhotra, A., Nikiforov, V., Goldfarb, A., and Darst, S. A. (2000) *Science 289*, 619−625.
8. Rana, T. M., and Meares, C. F. (1990) *J. Am. Chem. Soc. 112*, 2457−2458.
9. Owens, J. T., Chmura, A. J., Murakami, K., Fujita, N., Ishihama, A., and Meares, C. F. (1998) *Biochemistry 37*, 7670−7675.
10. Owens, J. T., Miyake, R., Murakami, K., Chmura, A. J., Fujita, N., Ishihama, A., and Meares, C. F. (1998) *Proc. Natl. Acad. Sci. U.S.A. 95*, 6021−6026.
11. Traviglia, S. L., Datwyler, S. A., and Meares, C. F. (1999) *Biochemistry 38*, 4259−4265.
12. Traviglia, S. L., Datwyler, S. A., Yan, D., Ishihama, A., and Meares, C. F. (1999) *Biochemistry 38*, 15774−15778.
13. King, D. J., Ventura, D. A., Brasier, A. R., and Gorenstein, D. G. (1998) *Biochemistry 37*, 16489−16493.
14. Fidanza, J. A., and McLaughlin, L. W. (1989) *J. Am. Chem. Soc. 111*, 9117−9119.
15. Dervan, P. B. (1991) *Methods Enzymol. 208*, 497−515.
16. Zhang, G., Campbell, E. A., Minakhin, L., Richter, C., Severinov, K., and Darst, S. A. (1999) *Cell 98*, 811−824.
17. Malhotra, A., Severinova, E., and Darst, S. A. (1996) *Cell 87*, 127−136.
18. Greiner, D. P., Miyake, R., Moran, J. K., Jones, A. D., Negishi, T., Ishihama, A., and Meares, C. F. (1997) *Bioconjugate Chem. 8*, 44−48.
19. Tagami, H., and Aiba, H. (1995) *Nucleic Acids Res. 23*, 599−606.
20. Renn, O., Goodwin, D. A., Studer, M., Moran, J. K., Jacques, V., and Meares, C. F. (1996) *J. Controlled Release 39*, 239−249.
21. Harlow, E., and Lane, D (1988) in *Antibodies: A Laboratory Manual*, Cold Spring Harbor Laboratory Press, Cold Spring Harbor, NY.
22. Reardan, D. T., Meares, C. F., Goodwin, D. A., McTigue, M., David, G. S., Stone, M. R., Leung, J. P., Bartholomew, R. M., and Frincke, J. M. (1985) *Nature 316*, 265−268.
23. Igarashi, K., and Ishihama, A. (1991) *Cell 65*, 1015−1022.
24. Kajitani, M., and Ishihama, A. (1983) *Nucleic Acids Res. 11*, 3873−3888.
25. Kajitani, M., and Ishihama, A. (1983) *Nucleic Acids Res. 11*, 671−686.
26. Chamberlin, M. J. (1974) *Annu. Rev. Biochem. 43*, 721−775.
27. Greiner, D. P., Hughes, K. A., Gunasekera, A. H., and Meares, C. F. (1996) *Proc. Natl. Acad. Sci. U.S.A. 93*, 71−75.
28. Miyake, R., Murakami, K., Owens, J. T., Greiner, D. P., Ozoline, O. N., Ishihama A., and Meares, C. F. (1998) *Biochemistry 37*, 1344−1349.
29. Bornstein, P., and Bolian, G. (1977) *Methods Enzymol. 47*, 132−145.
30. Arthur, T. M., and Burgess, R. R. (1998) *J. Biol. Chem. 273*, 31381−31387.
31. Lischwe, M. A., and Sung, M. T. (1977) *J. Biol. Chem. 252*, 4976−4980.
32. Jin, D. J., and Gross, C. A. (1988) *J. Mol. Biol. 202*, 45−58.
33. Campbell, E. A., Korzheva, N., Mustaev, A., Murakami, K., Nair, S., Goldfarb, A., and Darst, S. A. (2001) *Cell 104*, 901−912.
34. Jeon, Y. H., Negishi, T., Shirakawa, M., Yamazaki, T., Fujita, N., Ishihama, A., and Kyogoku, Y. (1995) *Science 270*, 1495−1496.
35. Gaal, T., Ross, W., Blatter, E. E., Tang, H., Jia, X., Krishnan, V. V., Assa-Munt, N., Ebright, R. H., and Gourse, R. L. (1996) *Genes Dev. 10*, 16−26.
36. Murakami, K., Fujita, N., and Ishihama, A. (1996) *EMBO J. 15*, 4358−4367.
37. Ross, W., Aiyar, S. E., Salomon, J., and Gourse, R. L. (1998) *J. Bacteriol. 180*, 5375−5383.
38. Rudakova, E. A., Ivanovskaya, M. G., Kozlov, M. V., Khoretonenko, M. V., Oretskaya, T. S., and Nikiforov, V. G. (2000) *Biochemistry (Moscow) 65*, 640−650.
39. Finn, R. D., Orlova, E. V., Gowen, B., Buck, M., and van Heel, M. (2000) *EMBO J. 19*, 6833−6844.
40. Sharp, M. M., Chan, C. L., Lu, C. Z., Marr, M. T., Nechaev, S., Merritt, E. W., Severinov, K., Roberts, J. W., and Gross, C. A. (1999) *Genes Dev. 13*, 3015−3026.
41. Juang, Y. L., and Helmann, J. D. (1994) *J. Mol. Biol. 235*, 1470−1488.
42. Juang, Y. L., and Helmann, J. D. (1995) *Biochemistry 34*, 8465−8473.
43. Waldburger, C., Gardella, T., Wong, R., and Susskind, M. M. (1990) *J. Mol. Biol. 215*, 267−276.
44. Siegele, D. A., Hu, J. C., Walter, W. A., and Gross, C. A. (1989) *J. Mol. Biol. 206*, 591−603.
45. Daniels, D., Zuber, P., and Losick, R. (1990) *Proc. Natl. Acad. Sci. U.S.A. 87*, 8075−8079.

BI015582R